FOI
SWEDISH DEFENCE
RESEARCH AGENCY

FOI–R––0580––SE
September 2002
ISSN 1650-1942

Base Data Report

Magnus Berglund Anders Larsson

Initial Numerical Simulations of the Flow in a Closed Electrothermal-Chemical Bomb

Weapons and Protection
SE-147 25 TUMBA

SWEDISH DEFENCE RESEARCH AGENCY
Weapons and Protection
SE-147 25 TUMBA

FOI–R––0580––SE
September 2002
ISSN 1650-1942

Base Data Report

Magnus Berglund Anders Larsson

Initial Numerical Simulations of the Flow in a Closed Electrothermal-Chemical Bomb

Issuing organization Swedish Defence Research Agency Weapons and Protection SE-147 25 TUMBA	**Report number, ISRN** FOI–R––0580––SE	**Report type** Base data report
	Research area code Combat	
	Month, year September 2002	**Project no.** E2005
	Customers code Contracted research	
	Sub area code Weapons and protection	
Author/s (editor/s) Magnus Berglund, Anders Larsson	**Project manager** Elisabeth Bemm	
	Approved by Torgny Carlsson	
	Scientifically and technically responsible Christer Fureby	

Report title
Initial Numerical Simulations of the Flow in a Closed Electrothermal-Chemical Bomb

Abstract (not more than 200 words)
In the present report initial numerical simulations of the flow in a closed electrothermal-chemical bomb has been conducted. For reasons of simplicity, all electrical discharge phenomena has been neglected in the simulations; with the aim of pinpointing various flow features of the simplified configuration and to build a "road map" for further implementation and development. A discussion of the modifications needed for the inclusion of electrical phenomena is also given.

Keywords
Interior ballistics, numerical simulation, electrothermal-chemical, ETC

Further bibliographic information	**Language** English
ISSN 1650-1942	**Pages** p.vi+30
	Price acc. to pricelist **Security classification**

Utgivare
Totalförsvarets Forskningsinstitut – FOI
Vapen och skydd
147 25 TUMBA

Rapportnummer, ISRN
FOI–R––0580––SE

Klassificering
Underlagsrapport

Forskningsområde
Bekämpning

Månad, år
September 2002

Projektnummer
E2005

Verksamhetsgren
Uppdragsfinansierad verksamhet

Delområde
VVS med styrda vapen

Författare/redaktör
Magnus Berglund, Anders Larsson

Projektledare
Elisabeth Bemm

Godkänd av
Torgny Carlsson

Tekniskt och/eller vetenskapligt ansvarig
Christer Fureby

Rapportens titel (i översättning)
Inledande numeriska simuleringar av strömningen i en sluten elektrotermisk-kemisk bomb

Sammanfattning (högst 200 ord)
Inledande numeriska simuleringar av strömningen i en sluten elektrotermisk-kemisk bomb har genomförts. För enkelhets skull har alla elektriska urladdningsfenomen försummats i simuleringen; detta för att fastslå vissa strömningsegenskaper hos den förenklade konfigurationen och för att skapa en "snitslad bana" för vidare implementationsutveckling. En diskussion ges också om de nödvändiga modifieringar som behövs för att inkludera elektriska urladdningsfenomen.

Nyckelord
Innerballistik, numerisk simulering, elektrotermisk-kemisk, ETC

Övriga bibliografiska uppgifter

Språk Engelska

ISSN 1650-1942

Antal sidor s.vi+30

Distribution enligt missiv

Pris: Enligt prislista

Sekretess

Contents

1 Introduction

The topic of this report is the present capability to computationally simulate closed bomb firings based on an extension of the model presented in [5]. The simulations described in this report is also fundamental for further development of the computer code to also include electric discharge phenomena, which is necessary for simulating systems that use an electrothermal-chemical (ETC) concept, as well as for studying the effects of the usage of different numerical schemes, different combustion models, and couplings in the combustion–acoustics–turbulence-system.

For the computation of turbulent fluid flows there are conceptually three different approaches: Reynolds-Averaged Numerical Simulation (RANS) in which only time mean quantities are computed[1] and all turbulence effects are modeled [31], Large Eddy Simulation (LES) where the large scales of the turbulent flow (termed the grid scale and abbreviated GS) are resolved while smaller scales (termed the subgrid scale and abbreviated SGS) are modeled, and Direct Numerical Simulation (DNS) where all length scales down to the Kolmogorov length scale are resolved, see e.g. [13]. In the two latter approaches one is also obliged to have a sufficient time resolution, and for many numerical solution practices this come in implicitly via stability criteria for the numerical schemes. For highly transient flows, modeling with RANS is not a candidate (at least as far as time-averaging is considered) and one should resort to either LES or DNS. Although DNS is the most accurate method it is prohibitively expensive in computer resources due to the high Reynolds number of the flow. The LES approach is, despite its relatively high computational demands, the best available alternative.

The report is organized as follows. Section 2 describes the flow modeling and the numerical methods used in this study. Section 3 is devoted to the specific simulations of a particular ETC bomb firing. An outlook of what can be done in forthcoming simulations and what has been omitted in this study is found in Section 4 and the conclusions round up this report in Section 5.

This report was typeset by $\mathcal{AMS}$-LaTeX, the LaTeX macro system of the American Mathematical Society.

[1] Sometimes the averaging is carried out over homogeneous directions or across an ensemble of equivalent flows, but time-averaging is by far the most commonly used practice

2 The Computational Approach

2.1 The Flow Modeling

As pointed out in e.g. [4] it is not generally possible to use an Eulerian approach, considering each phase as a continuum, for modeling interior ballistic flows. In the particular case of the ETC bomb, however, it is possible as there is only one propellant grain present. As this propellant grain is also pasted onto the inside of the bomb it is possible to use the same modeling principles as in [5]. As a few of the simplifying assumptions made in that work has been loosened, a brief survey of the modeling will now be given.

In the Eulerian approach it is necessary to construct a continuum representation of each phase, and this is most often done by performing a volume averaging, which we denote $\langle \cdot \rangle$, of the Navier–Stokes equations (NSE) for a single phase; considering each phase to be a single phase flowing "over" the other phases. This procedure gives, under the assumption that all phases can be considered to behave as Newtonian fluids[2] and that the external forces are negligible, a set of phase-averaged NSE for phase k (see e.g. [12]):

$$\begin{cases} \partial_t\langle\rho_k\rangle + \nabla\cdot\langle\rho_k\mathbf{u}_k\rangle = -\dfrac{1}{V}\displaystyle\int_{A_k}\rho_k(\mathbf{u}_k-\mathbf{u}_s)\cdot\mathbf{n}_k dA \\ \partial_t\langle\rho_k\mathbf{u}_k\rangle + \nabla\cdot\langle\rho_k\mathbf{u}_k\mathbf{u}_k\rangle = -\nabla\langle p_k\rangle + \nabla\cdot\langle\mathbf{S}_k\rangle \\ \qquad\qquad + \dfrac{1}{V}\displaystyle\int_{A_k}(-p_k\mathbf{1}+\mathbf{S}_k)\cdot\mathbf{n}_k dA \\ \qquad\qquad - \dfrac{1}{V}\displaystyle\int_{A_k}\rho_k\mathbf{u}_k(\mathbf{u}_k-\mathbf{u}_s)\cdot\mathbf{n}_k dA \\ \partial_t\langle\rho_k e_k\rangle + \nabla\cdot\langle\rho_k\mathbf{u}_k e_k\rangle = -\langle p_k\nabla\cdot\mathbf{u}_k\rangle - \nabla\cdot\langle\mathbf{j}_{q,k}\rangle + \langle j_{e,k}\rangle + \langle\phi_k\rangle \\ \qquad\qquad - \dfrac{1}{V}\displaystyle\int_{A_k}\mathbf{j}_{q,k}\cdot\mathbf{n}_k dA - \dfrac{1}{V}\int_{A_k}\rho_k e_k(\mathbf{u}_k-\mathbf{u}_s)\cdot\mathbf{n}_k dA \end{cases} \tag{2.1}$$

where ρ_k is the density of phase k, $\mathbf{u}_k$ the velocity of phase k, $\mathbf{u}_s$ is the velocity of the phase boundary, p_k the pressure of phase k, $\mathbf{S}_k = \eta_k(\operatorname{tr}\mathbf{D}_k)\mathbf{1} + 2\mu_k\mathbf{D}_{D,k}$, where $\mu_k = \rho_k\nu_k$ is the kinematic viscosity, η_k the bulk viscosity of phase k, $\mathbf{D}_{D,k} = \mathbf{D}_k - \frac{1}{3}(\operatorname{tr}\mathbf{D}_k)\mathbf{1}$ in which $\mathbf{D}_k = \frac{1}{2}(\mathbf{L}_k + \mathbf{L}_k^T)$ with $\mathbf{L}_k = \nabla\mathbf{u}_k$, e_k the specific internal energy of phase k, $\mathbf{j}_{q,k} = \hat{\kappa}_k\nabla e_k$ with $\hat{\kappa}_k$ the thermal conductivity (assuming Fourier heat conduction), $j_{e,k}$ the rate of heat generation per unit volume, and ϕ_k the dissipation. The volume of the full system is denoted by V and the integrals represent the rate of mass generation

[2] This assumption poses no restriction on the solid in the ETC bomb case, as will be seen on page 5.

of phase k per unit volume, transfer of pressure and viscous stresses, transfer of momentum, transfer of heat, and transfer of internal energy across the phase boundary per unit volume, respectively. The interfacial area of phase k is denoted A_k.

As the phase-averaged Eqs. (2.1) does not reflect the physical properties, but rather pseudoproperties, they must be recasted. A way to proceed is now to define intrinsic averages, which we denote $\langle\cdot\rangle_i$, by $\langle\psi_k\rangle = \alpha_k\langle\psi_k\rangle_i$ where α_k is the volume fraction of phase k. On introducing Favré-averaged quantities $\widetilde{\langle\psi_k\rangle}_i = \langle\rho_k\psi_k\rangle_i/\langle\rho_k\rangle_i$ and defining the sub-averaging volume scale (SAVS) quantities

$$\begin{aligned}
\mathbf{X}_k &= \langle\rho_k\rangle_i\Big(\widetilde{\langle\mathbf{u}_k\mathbf{u}_k\rangle}_i - \widetilde{\langle\mathbf{u}_k\rangle}_i\widetilde{\langle\mathbf{u}_k\rangle}_i\Big),\\
\xi_k &= \langle p_k\nabla\cdot\mathbf{u}_k\rangle_i - \langle p_k\rangle_i\nabla\cdot\widetilde{\langle\mathbf{u}_k\rangle}_i, \text{ and}\\
\mathbf{z}_k &= \langle\rho_k\rangle_i\Big(\widetilde{\langle\mathbf{u}_k e_k\rangle}_i - \widetilde{\langle\mathbf{u}_k\rangle}_i\widetilde{\langle e_k\rangle}_i\Big),
\end{aligned}$$

straightforward computations give

$$\begin{cases}
\partial_t\big(\alpha_k\langle\rho_k\rangle_i\big) + \nabla\cdot\Big(\alpha_k\langle\rho_k\rangle_i\widetilde{\langle\mathbf{u}_k\rangle}_i\Big) = -\dfrac{1}{V}\displaystyle\int_{A_k}\rho_k(\mathbf{u}_k-\mathbf{u}_s)\cdot\mathbf{n}_k dA\\
\partial_t\Big(\alpha_k\langle\rho_k\rangle_i\widetilde{\langle\mathbf{u}_k\rangle}_i\Big) + \nabla\cdot\Big(\alpha_k\langle\rho_k\rangle_i\widetilde{\langle\mathbf{u}_k\rangle}_i\widetilde{\langle\mathbf{u}_k\rangle}_i\Big) = -\nabla\big(\alpha_k\langle p_k\rangle_i\big)\\
\qquad\qquad + \nabla\cdot\Big(\alpha_k\big(\langle\mathbf{S}_k\rangle_i - \mathbf{X}_i\big)\Big) + \dfrac{1}{V}\displaystyle\int_{A_k}(-p_k\mathbf{1}+\mathbf{S}_k)\cdot\mathbf{n}_k dA\\
\qquad\qquad - \dfrac{1}{V}\displaystyle\int_{A_k}\rho_k\mathbf{u}_k(\mathbf{u}_k-\mathbf{u}_s)\cdot\mathbf{n}_k dA\\
\partial_t\Big(\alpha_k\langle\rho_k\rangle_i\widetilde{\langle e_k\rangle}_i\Big) + \nabla\cdot\Big(\alpha_k\langle\rho_k\rangle_i\widetilde{\langle\mathbf{u}_k\rangle}_i\widetilde{\langle e_k\rangle}_i\Big) = \alpha_k\xi_k\\
\qquad\qquad - \alpha_k\langle p_k\rangle_i\nabla\cdot\widetilde{\langle\mathbf{u}_k\rangle}_i - \nabla\cdot\Big(\alpha_k\big(\langle\mathbf{j}_{q,k}\rangle_i + \mathbf{z}_k\big)\Big)\\
\qquad\qquad + \alpha_k\langle j_{e,k}\rangle_i + \alpha_k\langle\phi_k\rangle_i\\
\qquad\qquad - \dfrac{1}{V}\displaystyle\int_{A_k}\mathbf{j}_{q,k}\cdot\mathbf{n}_k dA - \dfrac{1}{V}\displaystyle\int_{A_k}\rho_k e_k(\mathbf{u}_k-\mathbf{u}_s)\cdot\mathbf{n}_k dA
\end{cases} \tag{2.2}$$

It is instructive to look at these equations for the special case of only one present phase as they then are analogous to the low-pass filtered NSE as often used in LES. The SAVS terms thus correspond to the subgrid stress tensor, the subgrid pressure dilatation, and the subgrid energy flux vector, respectively, in LES terminology. For LES, these subgrid quantities must be modeled to close the equations as they, in general, are nonzero. Aspects on the modeling of these quantities can be found in e.g. [10, 11, 18, 25,

28, 29, 30]. In the case of the volume-averaged equations, however, the following heuristic reasoning applies: The SAVS quantities can essentially be written $\frac{1}{V}\int_V \psi^2 dV' - (\frac{1}{V}\int_V \psi dV')(\frac{1}{V}\int_V \psi dV')$ which, by the mean value theorem of integral calculus, equals $\psi^2(\mathbf{r}') - \psi^2(\mathbf{r}'')$ for some $\mathbf{r}', \mathbf{r}'' \in V$. If one in the succeeding discretization of the governing equations uses small enough finite volumes, the SAVS quantities are made negligibly small in comparison with the other terms. We boldly assume that this is always done at the discretization stage and thus we neglect the possible influences of these quantities.

Consider a special case with two phases where it is assumed that $\widetilde{\langle \mathbf{u}_2 \rangle_i} \equiv \mathbf{0}$ and that $\widetilde{\langle \mathbf{u}_1 \rangle_i} = \mathbf{0}$ in averaging volumes that contain some part of the phase boundary, thus implying that $\widetilde{\langle \mathbf{u}_2 \rangle_i} = \widetilde{\langle \mathbf{u}_1 \rangle_i}$ where $\alpha_2 = 1$ and on the phase boundary. This is the further assumption that is needed to be able to consider the solid to behave as a Newtonian fluid. This also imply that the subscripts on the velocities and velocity-dependent quantities are redundant and these are thus omitted where directly applicable. By further assuming that the two phases are in local thermodynamic equilibrium with each other (implying that no Newtonian heat convection occur), and that phase two is incompressible, straightforward calculations give, on noting that $\alpha_1 + \alpha_2 = 1$ and defining

$$
\begin{aligned}
\langle \rho \rangle_i &= (1-\alpha_2)\langle \rho_1 \rangle_i + \alpha_2 \langle \rho_2 \rangle_i, \\
\langle p \rangle_i &= (1-\alpha_2)\langle p_1 \rangle_i + \alpha_2 \langle p_2 \rangle_i, \text{ and} \\
\langle \rho e \rangle_i &= (1-\alpha_2)\langle \rho_1 e_1 \rangle_i + \alpha_2 \langle \rho_2 e_2 \rangle_i,
\end{aligned}
$$

$$
\left\{
\begin{aligned}
&\partial_t \langle \rho \rangle_i + \nabla \cdot \left(\langle \rho \rangle_i \widetilde{\langle \mathbf{u} \rangle_i} \right) = 0 \\
&\partial_t \left(\langle \rho \rangle_i \widetilde{\langle \mathbf{u} \rangle_i} \right) + \nabla \cdot \left(\langle \rho \rangle_i \widetilde{\langle \mathbf{u} \rangle_i} \widetilde{\langle \mathbf{u} \rangle_i} \right) = -\nabla \langle p \rangle_i + \nabla \cdot \langle \mathbf{S} \rangle_i \\
&\qquad + \frac{1}{V} \int_{A_1} \mathbf{S}_1 \cdot \mathbf{n}_1 dA \\
&\partial_t \left(\langle \rho \rangle_i \widetilde{\langle e \rangle_i} \right) + \nabla \cdot \left(\langle \rho \rangle_i \widetilde{\langle \mathbf{u} \rangle_i} \widetilde{\langle e \rangle_i} \right) = -\langle p \rangle_i \nabla \cdot \widetilde{\langle \mathbf{u} \rangle_i} \\
&\qquad - \nabla \cdot \left(\alpha_1 \langle \mathbf{j}_{q,1} \rangle_i + \alpha_2 \langle \mathbf{j}_{q,2} \rangle_i \right) + \alpha_1 \langle j_{e,1} \rangle_i + \alpha_1 \langle \phi_1 \rangle_i \\
&\qquad + \alpha_2 \langle j_{e,2} \rangle_i + \alpha_2 \langle \phi_2 \rangle_i - \frac{1}{V}(\kappa_1 - \kappa_2) \int_{A_1} \nabla T \cdot \mathbf{n}_1 dA \\
&\qquad - \frac{1}{V} \int_{A_1} (\rho_2 e_2 - \rho_1 e_1) \mathbf{u}_s \cdot \mathbf{n}_1 dA \\
&\partial_t \alpha_2 = -\frac{1}{V} \int_{A_1} \mathbf{u}_s \cdot \mathbf{n}_1 dA
\end{aligned}
\right. \tag{2.3}
$$

where $\langle \mathbf{S} \rangle_i = \alpha_1 \langle \mathbf{S}_1 \rangle_i + \alpha_2 \langle \mathbf{S}_2 \rangle_i$. The first three equations stem from adding the equations of conservation of mass, momentum, and energy for the two phases, respectively, and the fourth is simply the conservation of mass equation for phase two. It is interesting to note the similarity with the flow equations from mixture theory, see e.g. [8], where it is often assumed that the constituents have the same velocity. Although the same assumption, at least partly, is used here, it is the zero-velocity condition on phase two that makes it possible to identify the velocities $\widetilde{\langle \mathbf{u}_1 \rangle_i}$ and $\widetilde{\langle \mathbf{u}_2 \rangle_i}$ on subdomains where $\alpha_2 = 1$.

By reformulating the conservation of energy equation (2.3_3) to a conservation of enthalpy equation by the relations

$$\widetilde{\langle e \rangle_i} = \widetilde{\langle h \rangle_i} - \langle p \rangle_i / \langle \rho \rangle_i$$

and the total time derivative of the pressure

$$\dot{\langle p \rangle_i} = \partial_t \langle p \rangle_i + \widetilde{\langle \mathbf{u} \rangle_i} \cdot \nabla \langle p \rangle_i$$

one obtain the following flow equations

$$\begin{cases} \partial_t \langle \rho \rangle_i + \nabla \cdot \left(\langle \rho \rangle_i \widetilde{\langle \mathbf{u} \rangle_i} \right) = 0 \\ \partial_t \left(\langle \rho \rangle_i \widetilde{\langle \mathbf{u} \rangle_i} \right) + \nabla \cdot \left(\langle \rho \rangle_i \widetilde{\langle \mathbf{u} \rangle_i} \widetilde{\langle \mathbf{u} \rangle_i} \right) = -\nabla \langle p \rangle_i + \nabla \cdot \langle \mathbf{S} \rangle_i \\ \qquad\qquad + \dfrac{1}{V} \displaystyle\int_{A_1} \mathbf{S}_1 \cdot \mathbf{n}_1 dA \\ \partial_t \left(\langle \rho \rangle_i \widetilde{\langle h \rangle_i} \right) + \nabla \cdot \left(\langle \rho \rangle_i \widetilde{\langle \mathbf{u} \rangle_i} \widetilde{\langle h \rangle_i} \right) = \dot{\langle p \rangle}_i \\ \qquad\qquad - \nabla \cdot \left(\alpha_1 \langle \mathbf{j}_{q,1} \rangle_i + \alpha_2 \langle \mathbf{j}_{q,2} \rangle_i \right) \\ \qquad\qquad + \alpha_1 \langle \phi_1 \rangle_i + \alpha_2 \langle \phi_2 \rangle_i \\ \qquad\qquad - \dfrac{1}{V} (\kappa_1 - \kappa_2) \displaystyle\int_{A_1} \nabla T \cdot \mathbf{n}_1 dA \\ \qquad\qquad - \dfrac{1}{V} \displaystyle\int_{A_1} (\rho_2 h_2 - \rho_1 h_1) \mathbf{u}_s \cdot \mathbf{n}_1 dA \\ \partial_t \alpha_2 = -\dfrac{1}{V} \displaystyle\int_{A_1} \mathbf{u}_s \cdot \mathbf{n}_1 dA \end{cases} \tag{2.4}$$

The last subequation is, by means of the quasi-stationary Saint Robert–Vieille burn law ($r = ap^n$), simplified to

$$\partial_t \alpha_2 = -\frac{a}{V} \int_{A_1} \langle p \rangle_i^n dA$$

where a is the burning coefficient and n is the burning exponent and the integral source term in the enthalpy equation reduces to

$$-\frac{a}{V}\int_{A_1}(\rho_2 h_2 - \rho_1 h_1)\langle p\rangle_i^n dA.$$

The equation of state that is used to close the set of equations is a fourth-order accurate Boltzmann virial expansion, see e.g. [3], for a hard sphere-model of the gas molecules.

2.2 The Numerical Method

In conventional LES the flow is separated into small and large eddies by means of a low-pass filter, e.g. formulated as an integral filter or as a projection onto a finite set of basis functions, and equations for the latter are solved. To close the conventional LES equations and to emulate the effects of the SGS flow on the GS flow a certain extent of modeling is necessary. A lot of research has been done on SGS modeling and the models used are mostly Eddy Viscosity Models [17]. Formal drawbacks of conventional LES models are for example the assumption that the commutation error between the low-pass filtering and differentiation is negligible or can be modeled, the possible masking of SGS flux terms by leading order truncation errors, as well as general difficulties associated with formulating SGS models. In contrast to the conventional approach, in which the effects of the SGS flow on the GS flow are explicitly modeled, the recent alternative MILES (Monotone Integrated LES) [15, 16] uses the intrinsic properties of high-resolution schemes [20] to construct implicit (or built-in) SGS models by means of the leading order truncation errors, which can be shown to have properties similar to those of explicit models [15, 16]. Fundamental to MILES is the conceptual interpretation of turbulence as composed of thin filaments of intense vorticity embedded in a background of weak vorticity, see e.g. [23].

MILES draws on the observation that finite difference, finite volume, and finite element methods filter the equations to be solved over cells V_P, with characteristic dimension $|\mathbf{d}|$ — using an anisotropic top-hat shaped kernel

$$f_P = \tfrac{1}{V_P}\int_{V_P} f\, dV.$$

The discretized MILES equations can be obtained directly by applying some

particular discretization scheme to Eq. (2.4) and using Gauss's theorem

$$
\begin{cases}
\displaystyle\sum_{j=0}^{m}\Big(\gamma_j\big(\langle\rho\rangle_i\big)_P^{s+j}+\frac{\beta_j\Delta t}{V_P}\sum_f\Big(F_f^{C,\langle\rho\rangle_i}\Big)^{s+j}\Big)=0\\
\displaystyle\sum_{j=0}^{m}\Big(\gamma_j\Big(\langle\rho\rangle_i\widetilde{\langle\mathbf{u}\rangle_i}\Big)_P^{s+j}+\frac{\beta_j\Delta t}{V_P}\sum_f\Big(\mathbf{F}_f^{C,u}+\mathbf{F}_f^{D,u}+\mathbf{F}_f^{1,u}+\mathbf{F}_f^{2,u}\Big)^{s+j}\Big)\\
\qquad=-\beta_j\Big(\mathcal{D}\big(\nabla\langle p\rangle_i\big)+\frac{1}{V_P}\mathcal{D}\big(\textstyle\int_{A_1}\mathbf{S}_1\cdot\hat{\mathbf{n}}_1dA\big)\Big)_P^{s+j}\Delta t\\
\displaystyle\sum_{j=0}^{m}\Big(\gamma_j\Big(\langle\rho\rangle_i\widetilde{\langle h\rangle_i}\Big)_P^{s+j}+\frac{\beta_j\Delta t}{V_P}\sum_f\Big(F_f^{C,\widetilde{\langle h\rangle_i}}+F_f^{D,\widetilde{\langle h\rangle_i}}\Big)^{s+j}\Big)\\
\qquad=-\beta_j\Big(\alpha_1\langle\phi_1\rangle_i+\alpha_2\langle\phi_2\rangle_i-\frac{\kappa_1-\kappa_2}{V_P}\mathcal{D}\big(\textstyle\int_{A_1}\nabla T\cdot\hat{\mathbf{n}}_1dA\big)\\
\qquad\qquad-\frac{a}{V_P}\mathcal{D}\big(\textstyle\int_{A_1}(\rho_2h_2-\rho_1h_1)\langle p\rangle_i^ndA\big)\Big)_P^{s+j}\Delta t\\
\displaystyle\sum_{j=0}^{m}\gamma_j(\alpha_2)_P^{s+j}=-\beta_j\Big(\frac{a}{V_P}\mathcal{D}\big(\textstyle\int_{A_1}\langle p\rangle_i^ndA\big)\Big)_P^{s+j}\Delta t
\end{cases}
\tag{2.5}
$$

where $\mathcal{D}$ is some discretization operator, m, γ_j, and β_j are parameters of the scheme, and

$$
\begin{aligned}
F_f^{C,\langle\rho\rangle_i}&=\Big(\langle\rho\rangle_i\widetilde{\langle\mathbf{u}\rangle_i}\cdot d\mathbf{A}\Big)_f,\quad \mathbf{F}_f^{C,u}=\Big(\langle\rho\rangle_i\widetilde{\langle\mathbf{u}\rangle_i}\cdot d\mathbf{A}\Big)_f\Big(\widetilde{\langle\mathbf{u}\rangle_i}\Big)_f,\\
F_f^{C,\widetilde{\langle h\rangle_i}}&=\Big(\langle\rho\rangle_i\widetilde{\langle\mathbf{u}\rangle_i}\cdot d\mathbf{A}\Big)_f\widetilde{\langle h\rangle_i},\quad \mathbf{F}_f^{D,u}=\Big(\mu\mathcal{D}\Big(\nabla\widetilde{\langle\mathbf{u}\rangle_i}\Big)\Big)_f d\mathbf{A},\\
\mathbf{F}_f^{1,u}&=\Big(\lambda\mathcal{D}\Big(\nabla\cdot\widetilde{\langle\mathbf{u}\rangle_i}\Big)\Big)_f d\mathbf{A},\quad \mathbf{F}_f^{2,u}=\Big(\mu\mathcal{D}\Big(\nabla\widetilde{\langle\mathbf{u}\rangle_i}^T\Big)\Big)_f d\mathbf{A},\\
&\text{and } F_f^{D,\widetilde{\langle h\rangle_i}}=\Big(\frac{\kappa}{c_p}\mathcal{D}\Big(\nabla\widetilde{\langle h\rangle_i}\Big)\Big)_f\cdot d\mathbf{A}
\end{aligned}
$$

are the convective, viscous (diffusive), and auxiliary fluxes from the equations of conservation of mass, momentum, and enthalpy. Similar to conventional LES the discretization of inner derivatives must involve central differencing, whilst the functional reconstruction of the convective terms is designed to handle weak discontinuities (i.e. thin filaments of intense vorticity in a background of weak vorticity or shock-waves) effectively resulting in implicit SGS models. Such algorithms have to be nonlinear in order to comply with the physical principles of monotonicity, causality, and positivity [19]. A consistent way to derive such schemes is by using flux-limiters [7]. A flux-

limiter Γ is introduced to combine a high-order flux-function $\mathbf{v}_f^H$, that is well-behaved in smooth regions, with a low-order dispersion-free flux-function $\mathbf{v}_f^L$, being well-behaved near sharp gradients, so that the combination becomes $\mathbf{v}_f = \mathbf{v}_f^H - (1-\Gamma)\big(\mathbf{v}_f^H - \mathbf{v}_f^L\big)$. Typically, $\mathbf{v}_f^H$ is obtained from a linear approximation whilst $\mathbf{v}_f^L$ is obtained from an upwind-biased piecewise constant approximation, *viz.*

$$\mathbf{F}_f^{C,u,H} = F_f^{C,\langle\rho\rangle_i}\left(l\left(\widetilde{\langle\mathbf{u}\rangle_i}\right)_P + (1-l)\left(\widetilde{\langle\mathbf{u}\rangle_i}\right)_N - \frac{1}{8}\mathbf{dd}\cdot\mathcal{D}\left(\nabla^2\widetilde{\langle\mathbf{u}\rangle_i}\right)\right),$$

$$\mathbf{F}_f^{C,u,L} = F_f^{C,\langle\rho\rangle_i}\left(\beta^+\left(\widetilde{\langle\mathbf{u}\rangle_i}\right)_P + \beta^-\left(\widetilde{\langle\mathbf{u}\rangle_i}\right)_N + (\beta^+-\beta^-)\mathcal{D}\left(\nabla\widetilde{\langle\mathbf{u}\rangle_i}\right)\cdot\mathbf{d}\right),$$

$$\text{and } \beta^{\pm} = \frac{1}{2}\frac{\left(\widetilde{\langle\mathbf{u}\rangle_i}\right)_f\cdot d\mathbf{A} \pm \left|\left(\widetilde{\langle\mathbf{u}\rangle_i}\right)_f\cdot d\mathbf{A}\right|}{\left|\left(\widetilde{\langle\mathbf{u}\rangle_i}\right)_f\cdot d\mathbf{A}\right|},$$

where l is the distance function and the terms

$$-\tfrac{1}{8}\left(\mathbf{dd}\cdot\nabla^2\widetilde{\langle\mathbf{u}\rangle_i}\right) \text{ and } (\beta^+-\beta^-)\mathcal{D}\left(\nabla\widetilde{\langle\mathbf{u}\rangle_i}\right)\cdot\mathbf{d}$$

represent the leading order truncation errors. The flux limiter is formulated as to allow as much as possible of the correction or antidiffusion term $\left(\mathbf{v}_f^H - \mathbf{v}_f^L\right)$ to be included without violating the principles of monotonicity, causality, or positivity. Although the choice of flux limiter is not trivial the intrinsic properties of these are well-known, i.e. Γ must be a positive function of the ratios of consecutive variations in the dependent variables and it should only deviate from unity in regions where the variable is close to an extremum or has sharp gradients. Several existing limiters will satisfy these conditions and one being the FCT limiter of Boris and Book [6], even though the one used in this study is due to Jasak [22].

The implicit SGS model can be derived by a direct computation, revealing that the discretization has introduced additional dissipative and dispersive terms. The effects of these terms have been discussed elsewhere [16] and are not studied here.

Comparative studies using conventional LES and MILES applied to compressible free shear flows have been undertaken [15, 16]. It was found that they both work well provided that (i) the cut-off wavenumber, $\mathbf{k}_C$, lies within the inertial subrange and (ii) the combined model–algorithm–discretization adequately can channel kinetic energy out of wavenumbers close to $\mathbf{k}_C$ to prevent energy buildup and aliasing. For high Reynolds number free shear flows, the comparisons indicate that MILES is generally not worse than conventional LES.

3 Closed Bomb Firing Simulations

Initial numerical simulations of the flow in an ETC bomb similar to the experimental one at FOI, see e.g. [2], have been performed. The differences between the experimental and computational configurations is that the electrodes and the high voltage insulation of Bakelite are omitted in this study. The simulations tries to mimic Experiment 41 in the ETC experiment test series, where the propellant is pasted inside the rectangular cavity.

The simulations are performed on a mesh consisting of about $2.2 \cdot 10^5$ cells, see Fig. 1, and the burning exponent and coefficient for the Saint Robert–Vieille burn law that has been used are set to $a = 1.533 \cdot 10^{-3}$ m/s and $n = 0.92$, based on data from Experiment 40.

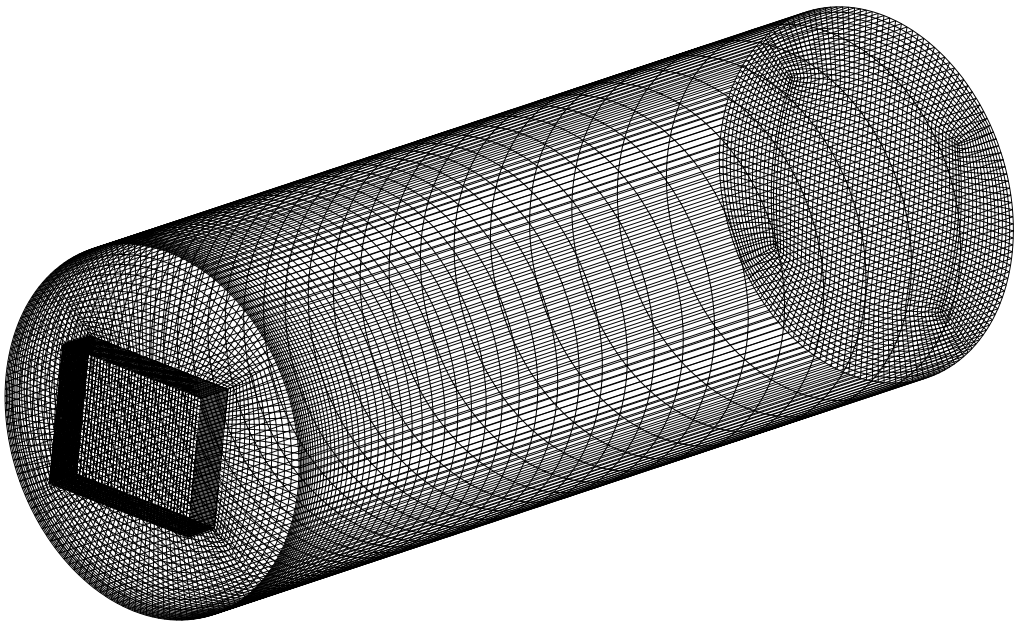

Figure 1: Perspective view of the boundary of the mesh used in this study.

The boundary conditions for this case can pose problems as all the boundaries are walls. The problem that can arise is that the pressure and temperature can start to "float" as the correct boundary condition to use is a zero gradient-condition and thus that there is no natural "level preserving" function for these quantities. The idea that has been employed in this work is to introduce an "artificial wall"-condition, where the pressure and temperature is kept fixed during each single time step but is permitted to vary between time steps. This approach has been proven useful for this type of flow.

The simulations are initialized with zero velocity throughout the computational domain and a uniform pressure of 102.87 MPa and a uniform temperature of 3 148 K in the gas phase. These pressure and temperature figures were computed with the thermo-chemistry computer code CEC93, see e.g. [14], for the specific kind and amount of booster propellant used in Experiment 41. The pressure and the temperature in the solid is initiated with a linear ramping function so that the end of the propellant that is farthest away from the gas–solid interface is at $p = 101.3$ kPa and $T = 300$ K, which is a pure (but probably poor) guess. A better approach could be to emulate the booster charge by "feeding" a cell somewhere in the gas volume with mass for some initial time. This will be examined in later studies.

The Euler implicit temporal discretization scheme has been used in this study as well as a few different time steps ranging between $2 \cdot 10^{-7}$ s and $1 \cdot 10^{-6}$ s. As the Euler implicit discretization scheme only is first-order accurate it is also of interest to use a higher-order scheme to find out if any pronounced differences arise or if a first order temporal discretization is sufficient. This issue will be addressed later. It was recognized that the pressure showed a step-like behavior at simulation restarts, and a subsequent oscillatory behavior. The origin of this was a minor programming error that now has been corrected. To get reasonable simulation data, these two "simulation restart"-jumps have been leveled out in Fig. 2 but the oscillations are still visible. It should also be noted in Fig. 2 that the initial pressure in the simulations are somewhat too high as compared to the experiment, being a potential source of errors.

In Fig. 3 the power spectral density (PSD) of the pressure is showed. The upper curve is computed from experimental data and the lower one from a virtual pressure probe in the simulation, located at the same position as the one used in the experiment. Although the power levels are quite different, it is comforting to see that the simulation has been able to find the peaks at about 4 300 Hz and 8 600 Hz from the experiment. As is often the case in this type of simulations, the time step used is so small that one obtain an, at least in some respects, unnecessarily large frequency range. The PSD from the simulation is based on a time interval of about 8.6 ms and a sampling

frequency of 5 MHz, which thus correspond to about 17.2 samples/kHz while the equivalent figure for the experiment is 138 samples/kHz. As too few samples per frequency unit give rise to an unwanted spectral broadening one is eager to decrease the sampling frequency, and it is possible that some minor modifications of the computer code can accomplish this without adding too large demands on the computational resources. This will be looked into in future studies.

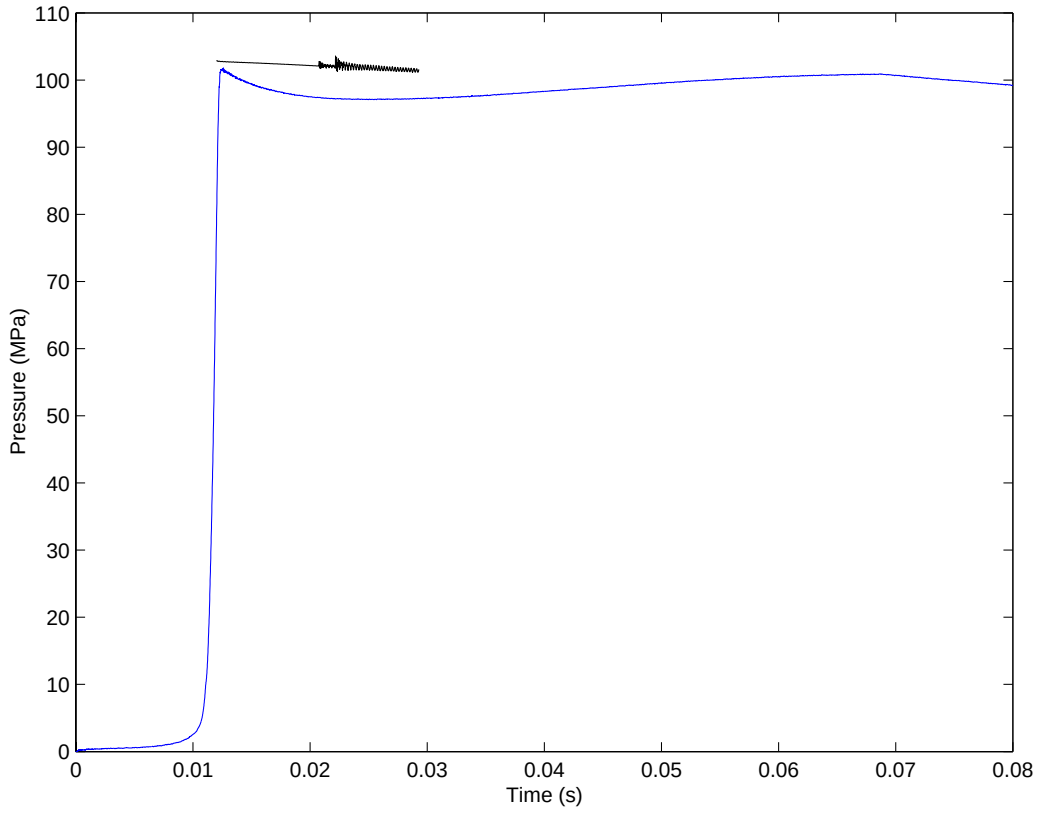

Figure 2: Time series of the pressure from calculation (black) and experiment (blue).

In Fig. 4 instantaneous velocity vectors colored with temperature on part of a center plane are shown. The temperature regime is between 500 K (blue) and 3 200 K (magenta) and the time elapsed between each frame is 1 ms. The occurrence of traveling waves is clearly visible in the bulk volume, even though the time elapsed between each panel is not optimal. The flow field in this volume is quite uniform, but in the vicinity of the propellant it is seen to be more complicated. As the propellant is consumed, and thereby

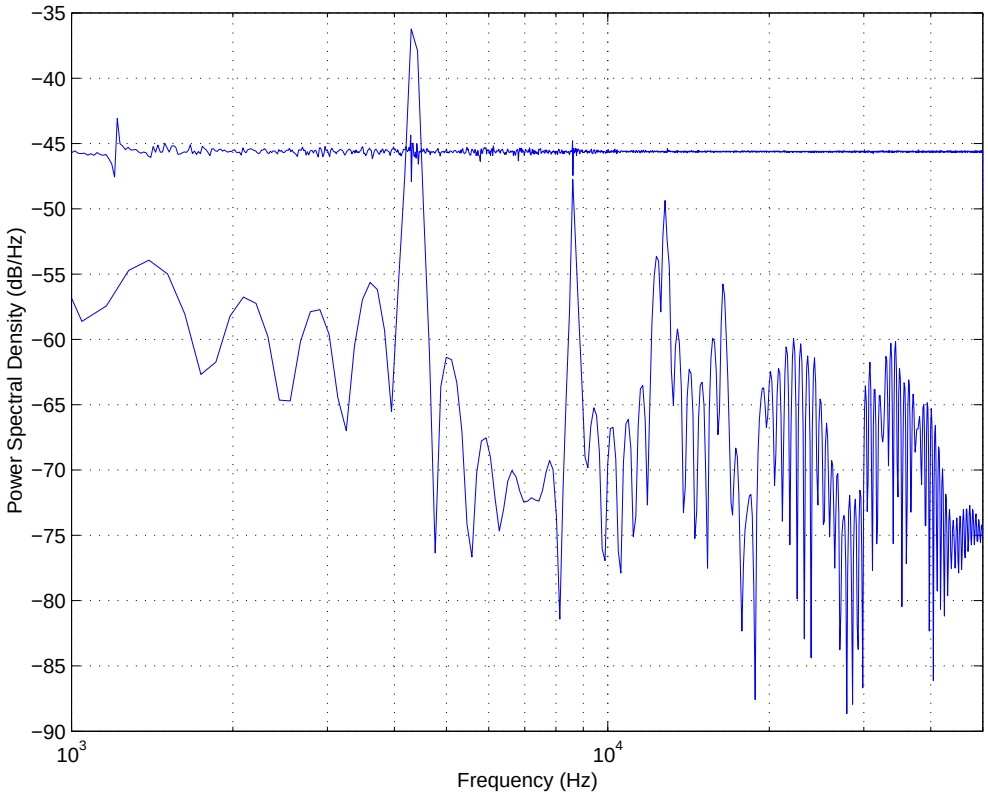

Figure 3: Power spectral density of pressure from calculation (lower curve) and experiment (upper curve).

releasing gas, the pressure gradient at the propellant surface can redirect the incoming bulk flow to an outgoing flow as seen in panels (e) and (f). In this redirection process, low-pressure regions are created above and under the "gas bursts" from the center of the propellant surface. This is clearly visible in all panels. As the combustion chamber is closed the outgoing flow will of course be reflected from the wall opposing the propellant, thus adding to the complexity of the flow and the combustion as it in this way is acoustically driven.

Figure 5 shows an instantaneous appearance of the propellant surface colored with temperature. The temperature range from 500 K (blue) to 1 500 K (magenta). As the amount of propellant in a computational cell is given as a volume fraction only, the propellant surface is represented as the iso-surface of the volume fraction equaling 0.5. From the faceted appearance of the pro-

pellant surface the immediate conclusion is that the mesh is not sufficiently resolved in the combustion zone. This must be remedied in further studies, but as the flow in the bulk of the combustion chamber seem to be adequately resolved it should be sufficient to use local mesh refinement in the rectangular cavity and in its immediate vicinity. It is also interesting to see that even though the combustion model that has been used is a quasi-stationary one, the propellant surface has nevertheless burnt in a fairly irregular way. Even though more intricate, and in general better, combustion models exist, see e.g. [4], this type of modeling may be sufficient if the nonlinear couplings from the flow and the acoustics dominate over the nonlinearities inherent in the combustion itself.

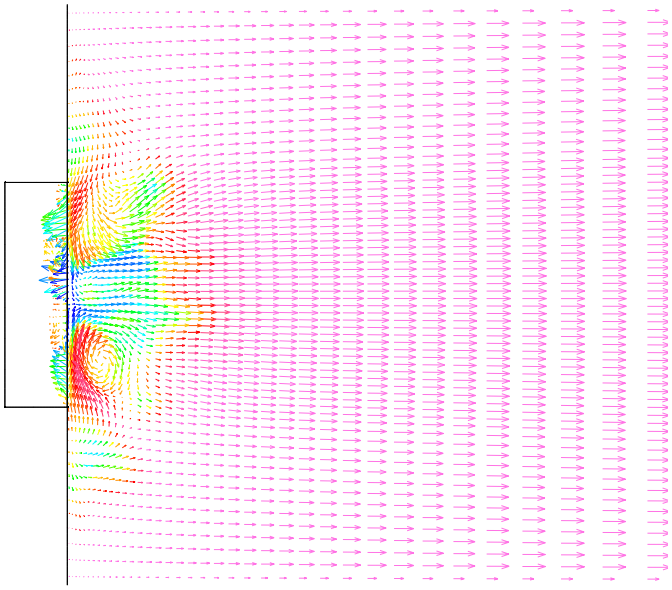

(a)

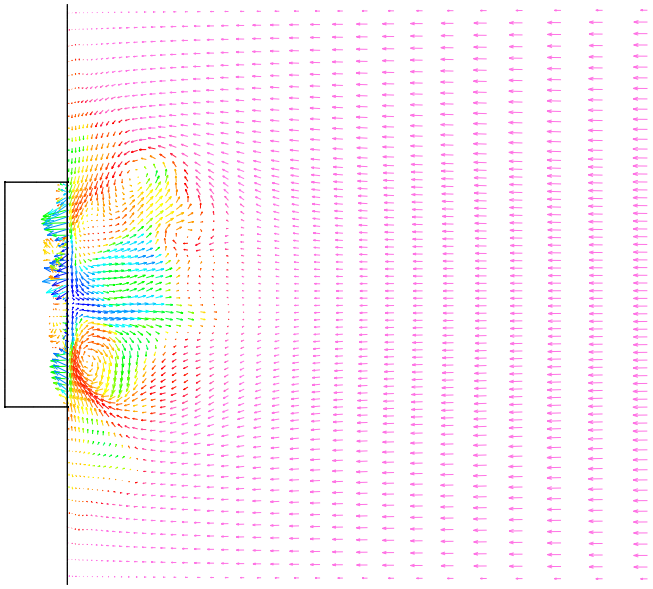

(b)

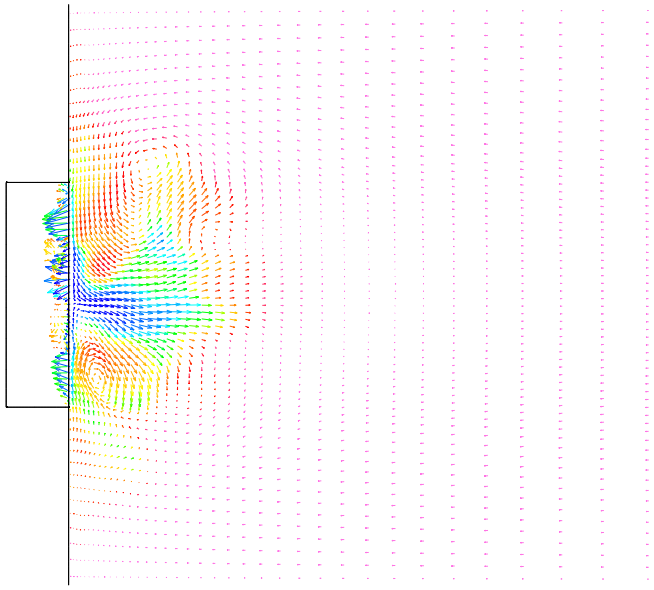

(c)

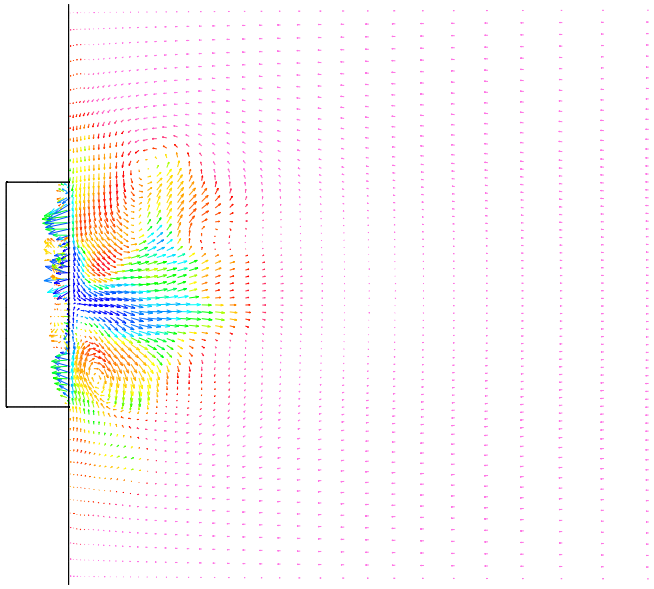

(d)

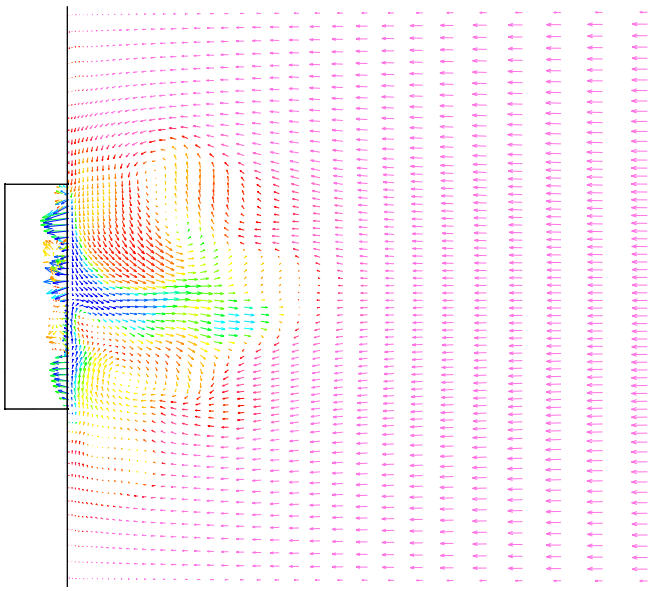

(e)

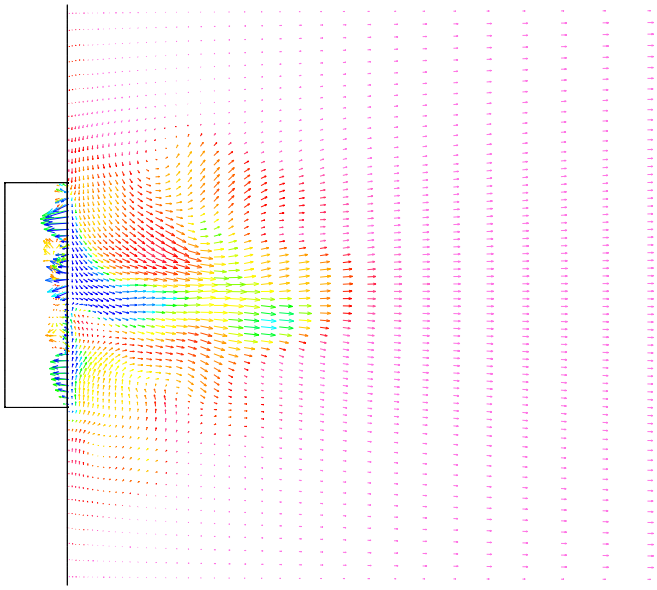

(f)

Figure 4: Instantaneous velocity vectors on part of a centerplane, vectors colored with temperature. The temperature regime is between 500 K (blue) and 3200 K (magenta) and the time elapsed between each frame is 1 ms.

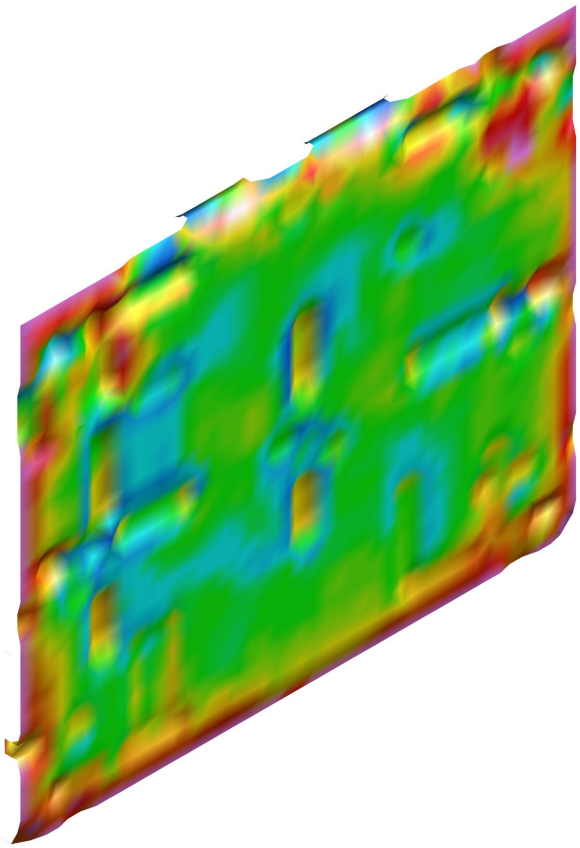

Figure 5: Instantaneous appearance of the propellant surface colored with temperature. The temperature range from 500 K (blue) to 1 500 K (magenta).

4 Omissions and Outlook

The central idea of FOI's ETC concept is to drive an electrical current through the combustion volume, thereby depositing electric energy in it to be able to modulate the temperature and pressure in the combustion zone. In order to account for the effects of an electric current, Eqs. (2.4) has to be modified. Here follows an outline of the modifications that are required. This material is mainly taken from Wangsness [32] and Jackson [21], unless otherwise stated.

To account for the energy transfer from a current that is driven through the combustion volume, two terms must be added to the right-hand side of the energy equation: the Joule heating term and the radiation term. The Joule heating term P_J is simply given by $P_J = \mathbf{j} \cdot \mathbf{E}$ where $\mathbf{j}$ is the current density and $\mathbf{E}$ the electric field strength. The radiation term S_r contains both radiation of electromagnetic energy and absorption of it [1, 9]. Thus, it is appropriate to split this term as $S_r = -S_{rad} + S_{abs}$ where S_{rad} and S_{abs} are radiation and absorption of electromagnetic energy, respectively. If assuming that the speed of light is infinite[3], the absorption term gives a non-local contribution to the local energy balance according to

$$S_{abs}(\mathbf{r}') = \int_V k\, S_{rad}(\mathbf{r}) \exp\left(-k|\mathbf{r} - \mathbf{r}'|\right) dV \tag{4.1}$$

where k is the absorption coefficient. The radiation from an electrical discharge is in non-equilibrium and origins mainly from free–free transitions (retardation radiation or bremsstrahlung) and from free–bound transitions (recombination radiation). To be complete, the energy equation ought to also contain the energy stored in the electromagnetic field w_{em} as given by

$$w_{em} = \frac{1}{2}(\mathbf{E} \cdot \mathbf{D} + \mathbf{H} \cdot \mathbf{B}) = \frac{1}{2}\left(\varepsilon_0 E^2 + \frac{1}{\mu_0} B^2\right).$$

This term is often neglected in models of discharge channels.

The right-hand side of the momentum equation must be completed with the electromagnetic force; the Lorentz force. The Lorentz force per unit volume $\mathbf{f}_{em}$ can be written as $\mathbf{f}_{em} = q\mathbf{E} + \mathbf{j} \times \mathbf{B}$ where $\mathbf{B}$ is the magnetic flux density. After a few manipulations, this force can be written as

$$\mathbf{f}_{em} = \nabla \cdot \mathbf{T}_{em} - \frac{\partial}{\partial t}(\mathbf{D} \times \mathbf{B})$$

[3]For a numerical simulation, this assumption implies that the time it takes for electromagnetic radiation to cross the computational volume is significantly smaller than the smallest time step used in the simulation.

where $\mathbf{T}_{em}$ is the Maxwell stress tensor and $\mathbf{D}$ is the electric displacement field. Another way of representing the Lorentz force is to introduce its effect as a momentum density of the electromagnetic field as $\mathbf{p}_{em} = \mathbf{D} \times \mathbf{B}$.

In principle, the mass equation already contains all species, including ions and electrons. However, the charged species require special attention since they carry the conduction current.

To close the set of equations, one may use Ohm's law $\mathbf{j} = \sigma\mathbf{E}$, where σ is the electrical conductivity, and one of Maxwell's equations

$$\nabla \times \mathbf{B} = \mu_0 \left(\mathbf{j} + \frac{\partial \mathbf{D}}{\partial t} \right).$$

To facilitate the solution of the system of equations and the choice of proper boundary conditions, one often define the electric scalar potential ϕ_{el}[4] and the magnetic vector potential $\mathbf{A}$ according to

$$\begin{aligned} \mathbf{E} &= -\nabla\phi_{el} - \frac{\partial \mathbf{A}}{\partial t} \\ \mathbf{B} &= \nabla \times \mathbf{A} \end{aligned}$$

One topic that must be appreciated in the study of electrical discharges is the processes at the electrodes [27]. In particular, the cathode processes play a major role in the discharge since the current-carrying electrons must be extracted from it into the gas discharge gap. The situation at the anode is simpler; here the electrode "only" has to collect the electrons, even if the bombardment of negative ions may be important. For an electron to escape from a metal surface, it must overcome the potential barrier of the surface. There are mainly three mechanisms for electron emission from metal surfaces:

- Thermionic emission
- Field emission
- Secondary emission

The thermionic emission is based on the fact that at non-zero temperatures, a few electrons possess sufficient energy to escape from the potential well formed by the metal. The current density extracted from the surface can be calculated by the Richardson–Dushman equation

$$j = CT^2 e^{-\Phi/(k_B T)}$$

[4]The electric scalar potential is usually denoted ϕ, but to avoid a possible name conflict with the dissipation term in Eqs. (2.1)–(2.4) an index is used.

where C is a constant, T is the temperature, Φ is the work function of the metal, and k_B is Boltzmann's constant. In experiments, it has been observed that the factor C is often considerably smaller than the expected value. The explanation is found in quantum mechanics: even though an electron may possess sufficient energy to escape from the well, there is a non-zero probability for it to be reflected back into the material. If the surface is subjected to a weak electric field, the potential energy barrier is lowered and thus decreases the effective work function. This is known as the Schottky effect.

If the electric field is strong, field emission occur. Field emission is the quantum mechanic tunneling of the electrons out of the metal surface. For electrical discharges such as glow and arc discharges, the thermionic emission dominates over the field emission.

Secondary emissions from electrode surfaces are very important. The term covers, however, a wide variety of processes and can be defined as in [26]

> *When a source of charged particles is dependent on another source of ionisation or excitation within the discharge it is termed a secondary effect.*

Among the secondary emission mechanisms one can mention photoelectric emission and emission caused by bombardment of positive ions and by metastable molecules.

For solving the equation system outlined above requires knowledge about the following properties:

- Electric conductivity
- Permittivity and permeability
- Radiation and absorption coefficients

Both the electrical conductivity and the radiation/absorption can be obtained by direct experimental curves or by refined models of desired degree and complexity. This decision must be made in each individual implementation of the global equation system. However, one should always bear in mind that the use of analytical expressions or complex models in discharge physics modeling not always show to be more reliable than a direct specification of the dependence based on existing experimental data [24].

Concerning the implementation, these issues are the most prominent and fortunately they will probably not give rise to any severe difficulties. The implementation of the radiation absorption term, Eq. (4.1), is probably the most critical as it potentially is computationally expensive.

5 Concluding Remarks

In this study initial numerical simulations of the flow in a closed electro-thermal-chemical bomb has been conducted. For simplicity, all electrical discharge phenomena has been neglected in the simulations; with the aim of pinpointing various flow features of the simplified configuration as well as for building a "road map" for further implementation development. A discussion of the modifications needed for the inclusion of electrical phenomena is also given. To evaluate the simulations we have tried to mimic Experiment 41 in the ETC experiment test series, where no electrical discharges were used. The results from the simulations have given useful knowledge about the type of flowfield that can be expected for such a configuration as well as listing of issues to include in the implementation "road map". The itemized conclusions is as follows:

- The "artificial wall"-condition, where the pressure and temperature is kept fixed during each single time step but is permitted to vary between time steps, has been proven useful for this type of flow.
- The initial conditions that has been used are too harsh and a better approach could be to emulate the booster charge by "feeding" a cell somewhere in the gas volume with mass for some initial time.
- The mesh is not sufficiently resolved in the combustion zone.

In future studies we are going to consider the following issues:

- Several meshes should be used and in particular one should strive to get a better resolution in the combustion zone. As the flow in the bulk of the combustion chamber seem to be adequately resolved it should be sufficient to use local mesh refinement in the rectangular cavity and in its immediate vicinity.
- Evaluate the use of higher-order temporal schemes to find out if any pronounced differences arise or if a first order discretization is sufficient.
- The initial conditions should be modified to closer mimic the actual experiment and an applicable approach could be to emulate the booster charge by "feeding" a cell somewhere in the gas volume with mass for some initial time.
- Investigate if minor modifications of the computer code can accomplish more samples per frequency unit, in order to reduce the spectral broadening in the power spectral density plots from the simulations, without adding to large demands on the computational resources.

- Examine if the combustion modeling is sufficient, i.e. if the nonlinearities from the flow and the acoustics dominate over the nonlinearities inherent in the combustion itself, or if one should resort to more intricate models.
- Implement modifications to handle electrical phenomena described in Section 4.

References

[1] Akram, M., "Modeling of Spark to Ignition Transition in Gas Mixtures", PhD thesis, Division for Combustion Physics, Lund Institute of Technology, 1996.

[2] Andreasson, S., Bemm, E., and Nyholm, S.E., "Resultat och erfarenheter från forskningen inom ETK-området", FOI−R−−0299−−SE, FOI User Report, 2001. (In Swedish)

[3] Bauer, P., Brochet, C., Heuze, O., and Presles, H.N., "Equation of State for Dense Gases", *Arch. Comb.* **5**, 35 (1985).

[4] Berglund, M., "On the Development of a Computational Tool for Interior Ballistics Simulations", FOI−R−−0308−−SE, FOI Base Data Report, 2001.

[5] Berglund, M., and Fureby, C., "Large Eddy Simulation of the Flow in a Solid Rocket Motor", *AIAA Paper 2001-0895* (2001).

[6] Boris, J.P., and Book, D.L., "Flux Corrected Transport I, SHASTA, a Fluid Transport Algorithm that Works", *J. Comp. Phys.* **11**, 38 (1973).

[7] Boris, J.P., Grinstein, F.F., Oran, E.S., and Kolbe, R.J., "New Insights into Large Eddy Simulation", *Fluid Dyn. Res.* **10**, 199 (1992).

[8] Bowen, R.M., "Theory of Mixtures", In: Eringen, C., (ed.), *Continuum Physics*, Vol.2, Academic Press, New York, 1976.

[9] Braginskii, S.I., "Theory of the Development of a Spark Channel", *Soviet Physics JETP* **34**, 1068 (1958).

[10] Deardorff, J.W., "The Use of Subgrid Transport Equations in a Three-Dimensional Model of Atmospherical Turbulence", *J. Fluids Engng. Trans ASME* **95**, 429 (1973).

[11] Erlebacher, G., Hussaini, M.Y., Speziale, C.G., and Zang, T.A., "Toward the Large-Eddy Simulation of Compressible Turbulent Flows", *J. Fluid Mech.* **238**, 155 (1992).

[12] Fan, L.-S., and Zhu, C., *Principles of Gas–Solid Flows*, Cambridge Series in Chemical Engineering, Cambridge University Press, Cambridge, 1998.

[13] Ferziger, J.H., "Large Eddy Simulation", In: Gatski, T.B., Hussaini, M.Y., and Lumley, J.L. (eds.) *Simulation and Modeling of Turbulent Flows*, Oxford University Press, Oxford, 1996.

[14] Flygar, S.-E., "INCEC93, inläsningsprogram till termokemiprogrammet CEC93", FOA Report C 20973-2.1, 1994. (In Swedish)

[15] Fureby, C., and Grinstein, F.F., "Monotonically Integrated Large Eddy Simulation of Free Shear Flows", *AIAA J.* **37**, 544 (1999).

[16] Fureby, C., and Grinstein, F.F., "Large Eddy Simulation of High-Reynolds-Number Free and Wall-Bounded Flows", *J. Comp. Phys.* **181**, 68 (2002).

[17] Fureby, C., Tabor, G., Weller, H.G., and Gosman, A.D., "A Comparative Study of Subgrid Scale Models in Homogeneous Isotropic Turbulence", *Phys. Fluids* **9**, 1416 (1997).

[18] Fureby, C., Tabor, G., Weller, H.G., and Gosman, A.D., "On Differential Sub Grid Scale Stress Models in Large Eddy Simulations", *Phys. Fluids* **9**, 3578 (1997).

[19] Gudonov, S.K., "A Difference Method for Numerical Calculation of the Equations of Hydrodynamics", *Mat. Sb.* **47**, 271 (1959).

[20] Hirsh, C., *Numerical Computation of Internal and External Flows*, Wiley, Chichester, 1997.

[21] Jackson, J.D., *Classical Electrodynamics*, John Wiley & Sons, New York, 1975.

[22] Jasak, H., *Error Analysis and Estimation for the Finite Volume Method with Application to Fluid Flows*, PhD Thesis, Imperial College, London, 1997.

[23] Jimenez, J., "Kinematic Alignment Effects in Turbulent Flows", *Phys. Fluids* **A4**, 652 (1992).

[24] Lagarkov, A.N., and Rutkevich, I.M., *Ionasation Waves in Electrical Breakdown of Gases*, Springer, Berlin, 1993.

[25] Lesieur, M., and Metais, O., "New Trends in Large-eddy Simulations of Turbulence", *Annu. Rev. Fluid Mech.* **28**, 45 (1996).

[26] Little, P.F., "Secondary Effects", In: Flügge, S., (ed.), *Handbuch der Physik*, Springer, Berlin, 1954.

[27] Raizer, Yu. P., *Gas Discharge Physics*, Springer, Berlin, 1997.

[28] Rodi, W., "A New Algebraic Relation for Calculating the Reynolds Stresses", *ZAMM* **56**, 219 (1976).

[29] Schumann, U., "Subgrid Scale Model for Finite Difference Simulation of Turbulent Flows in Plane Channels and Annuli", *J. Comp. Phys.* **18**, 376 (1975).

[30] Smagorinsky, J., "General Circulation Experiments with the Primitive Equations. I. The Basic Experiment", *Month. Wea. Rev.* **91**, 99 (1963).

[31] Speziale, C.G., "Modeling of Turbulent Transport Equations", In: Gatski, T.B., Hussaini, M.Y., and Lumley, J.L. (eds.) *Simulation and Modeling of Turbulent Flows*, Oxford University Press, Oxford, 1996.

[32] Wangsness, R., *Electromagnetic Fields*, John Wiley & Sons, New York, 1979.